ISSN: 2993-8643

Research Article

Engineering: Open Access

# Numerical Study of Entropy Generation with Magnetohydrodynamics on Natural Convection in a Porous Medium using Lattice Boltzmann Method

**Dawda Charreh[1,3], Shams-ul-Islam[1], M. Saleem[2], Bai Mbye Cham[1,3]* and Shaiza Talib[1]**

*[1]Department of Mathematics, COMSATS University Islamabad, Tarlai Kalan, Pakistan.*

*[2]Department of Science and Humanities, Sir Syed CASE Institute of Technology, Pakistan.*

*[3]Department of Mathematics, University of The Gambia, Serrekunda, The Gambia*

***Corresponding Author**
Bai Mbye Cham, *Department of Mathematics, University of The Gambia, Serrekunda, The Gambia.*

**Submitted**: 2023, July 14; **Accepted**: 2023, Aug 26; **Published**: 2023, Aug 30

**Citation:** Charreh, D., Islam, S. U., Saleem, M., Cham, B. M., Talib, S. (2023). Numerical Study of Entropy Generation with Magnetohydrodynamics on Natural Convection in a Porous Medium using Lattice Boltzmann Method. *Eng OA, 1*(2), 75-89.

## Abstract

*The study seeks to presents numerically the heat transfer phenomenon using natural convection in porous media. A square enclosure (cavity) filled with a porous medium simulated through Lattice Boltzmann Method which was used to analysed its effect on Fluid flows. The Darcy Forcheimer model will be adopted to show transfer of heat on the porous media. Magnetic effect is considered by including a magnetic field in they-momentum equation. The effects by various dimensionless parameters on generation of entropy are efficiently analyzed. Results from the investigations show that the Darcy-Forcheimer and magnetic effect both have relevant impact on entropy in a porous medium. The Eckert number affects the energy conversion and dissipation mechanisms, which in turns affect the rate of entropy generation.*

**Keywords:** Lattice Boltzmann Method, Entropy Generation, Magnetohydrodynamics, Thermal Radiation.Future Prospects.

## 1 Introduction

Lattice Boltzmann Method (LBM) described as a recent technique for numerical simulations has proven to be accurate and efficient for ascertaining the effects of heat transfer on porous media. LBM is easy to create and parallelize, making it computationally efficient. Its lattice structure facilitates the simulation of complex fluid behaviours such as multiphase flows and fluid-structure interactions. Haghshenas et al [1]. presents a simulation study on an openended square cavity filled with porous medium using LBM on natural convection [2]. Venkatadri and B´eg shows an LBM for thermo-magnetic cavity problem in a porous system for natural convection. The authors present a comprehensive analysis of the numerical results, including flow patterns and thermal distribution for different values of magnetic field strength, porosity, and Rayleigh number. Yang et al [3]. proposed a unified LBM for solving partial differential equations. Yong et al [4]. studied LBM approach for determining function slope in relation to control parameters.

Magnetic effect can also play significant role on transfer of heat for a porous media, particularly in magnetohydrodynamics, magnetic refrigeration, and magnetic drug targeting. Including a magnetic field in the momentum equation can enhance or suppress fluid flows in porous medium. Geridonmez et al [5]. presents a natural convection in a square cavity filled with porosity on a partial magnetic field. Mahmoudi and Ahmed studied a scale analysis on porous medium in the presence of magnet for natural convection [6]. The aim of the investigation is to analysed the physical mechanisms that govern fluid flows on magnetic fields for a porous system. Jamshed et al [7]. shows that the inclusion of magnetic fields can improve heat transfer performance while decreasing system entropy generation. Tayebs et al [8]. give a thorough investigation of the effects of magnetic fields and fin geometry on the thermo-economic performance and entropy generation of natural convective flow in a fluid's circular enclosure. The work has crucial implications for building sustainable energy systems, demonstrating the potential of magnetic fields to improve natural convection heat transfer efficiency in such systems.

| Nomenclature | | | |
|---|---|---|---|
| $u$ | velocity along x component | $\rho$ | density |
| $v$ | velocity along y component | $\mu$ | dynamic viscosity |
| $x$ | x component | $C_P$ | specific heat |
| $y$ | y component | $k$ | Thermal conductivity |
| $p$ | Pressure | $K$ | permeability of the porous media |
| $T$ | local temperature | $d$ | mean particle diameter |
| $\epsilon$ | porosity | $F$ | form drag constant |
| $\beta$ | Thermal expansion coefficient | $g$ | gravitational acceleration |
| $\|V\|$ | velocity vector | $\sigma^*$ | Stefan-Boltzmann constant |
| $k'$ | absorption coefficient | $T_h$ | hot area at the boundary |
| $T_c$ | cold area at the boundary | $\omega$ | vortocity |
| $\psi$ | stream function | $\nu$ | Kinematic viscosity |
| $Ra$ | Rayleigh number | $\gamma$ | inverse Darcy number |
| $\Gamma$ | Forchheimer Number | $Gr$ | Grashof Number |
| $Da$ | Darcy number | $Rd$ | radiation parameter |
| $Ec$ | Eckert number | $Nu$ | Local Nusselt number |
| $Nu_{avg}$ | Average Nusselt number | $\alpha$ | Thermal diffusivity |
| $\theta$ | Dimensionless Temperature | $\Phi$ | Viscous dissipation |
| $S_H$ | Entropy due to heat | $S_F$ | Entropy due to fluid friction |
| $S_T$ | Total Entropy | $\Delta\theta$ | Temparature Difference |
| $q_{rx}$ | Radiation flux with respect to x | $q_{ry}$ | Radiation flux with respect to y |
| $q_r$ | Thermal Radiation | $\bar{t}$ | Dimensionless time |
| $\tau_f$ | relaxation time for velocity | $\tau_g$ | relaxation time for temperature |
| $f_i^{eq}(x,t)$ | equilibrium for velocity | $g_i^{eq}(x,t)$ | equilibrium for temperature |
| $f_i(x,t)$ | distribution for temperature at time t | $g_i(x,t)$ | distribution for velocity at time t |
| $\mathbf{u}$ | microscopic velocity | $c_s$ | speed of sound |
| $c_i$ | speed of lattice particles | $\triangle\, x$ | lattice space |
| $c_i$ | speed of lattice particles | $\triangle\, t$ | lattice space |
| $w_i$ | weight function | | |

Darcy Forchheimer commonly describe the transfer of momentum in porous media. It takesinto account the viscous drag forces exerted by some solid matrix on fluid flow. Fluid dynamics and heat transfer has create valuable contribution in recent findings, and it may have potential applications in various fields, including biomedical engineering and renewable energy. Rasool et al [9]. presents a numerical investigation of Darcy Forchheimer relation with Casson fluid magnetohydrodynamic nanofluid flow in a non-linear surface characterize by stretching. The authors aim to investigate the effect of various parameters like Casson, magnetic field and non-dimensional parameters on heat transfer characteristics in nanofluid. The paper provides valuable contribution on fluid dynamics and heat transfer for nanofluids under the effect of magnetic fields, and it may have potential applications in various fields, including propulsion and power systems. Loganathan et al [10]. aim to analyze the heat transfer and entropy generation in the presence of Darcy-Forchheimer porous media.

Entropy generation is a key topic in several scientific and technical domains, including thermodynamics, fluid mechanics, and information theory. It measures the irreversible and chaotic quality of processes and systems, representing total energy deterioration and loss of order. Shah et al [11]. investigates optimization of entropy in Darcy-Forchheimer magnetohydrodynamic flow with Joule heating and viscous dissipation. Hayat et al [12]. present an analysis of the numerical results, including effects of parameters on transfer of heat phenomena, as well as entropy generation. The authors also optimize the system for minimum entropy generation and discuss the significance of the results in understanding fluid dynamics and heat transfer chemical reactive Darcy-Forchheimer flow with magnetic field. The work presents a numerical investigation of the impact of entropy generation on the magnetic field in a square cavity filled with a binary mixture fluid subjected to thermosolutal convection. The paper employs computational tools to simulate the fluid and magnetic field behaviour, taking into consideration issues such as heat transfer and solute transport. The paper provides valuable insights into the effects of slip on

entropy generation in MHD flows, highlighting the potential for slip to reduce entropy generation in such systems [13, 14]. Consequently, Saleem et al [15]. discuss entropy generation in a marangoni flow and heat transfer process due to its irreversibility natural process, as stated on the second law of thermodynamics. Many factors of recent research have contributed greatly to the change in entropy, among which includes fluid flow friction, heat transfer mechanisms and process. Since entropy concentrate on how much thermal energy or heat is lost per temperature, we could observe its wide range of practical application on boiling water, popcorn making and ice melting [16-19]. Furthermore, Alzahrani et al [20]. aim to optimize the entropy generation of the fluid flows by applying a rotating disk. The study presents a comprehensive analysis of the numerical results, including some effects of various parameters such as magnetic field and bioconvection on fluid flow. Jawad et al. also worked on a similar area of study [21].

Natural convection for heat transfer Phenomena in a porous system has received numerous attention in recent years due to it's importance in various engineering applications, like geothermal energy extraction, underground heat storage, and building insulation. Numerical methods are essential tools to study such phenomena since analytical solutions are often not available. In this paper, the LBM is used to simulate heat transfer of natural convection in cavity filled with a porosity. Darcy-Forcheimer model and magnetic effect are included in the momentum equation and energy equations so as to assess the effect on the entropy generation. The results of this study will provide insights into the behavior of natural convection through a porous media and help analysed the massive effect of magnet on a porous media for heat transfer.

## 2 Mathematical Formulation

In the presence of an applied magnetic field, the flow is considered unsteady, laminar, and incompressible natural convection in a cavity filled with porous medium. The geometry of the problem is shown in Figure 1. The top and bottom walls are adiabatic, with the left wall considered hot (Th) and the right wall considered cold (Tc). The porous medium is isotropic and homogeneous. The Boussinesq model was buoyancy on the momentum equation, the thermophysical characteristics of the flow are assumed as constants. The magnetic field, viscous dissipation, and radiation effects are all inclusive and significant in the model.

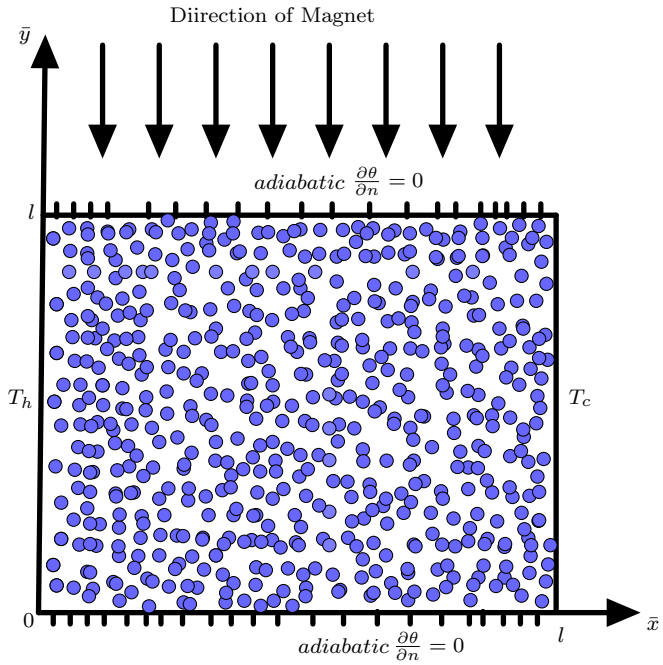


**Figure 1:** The Magnetic Direction, adiabatic process and definitions on the walls

Equation (1)-(4) presents the conservation of mass, momemtum and energy equation for a 2D cavity problem.

$$\frac{\partial u}{\partial x}+\frac{\partial v}{\partial y}=0 \tag{1}$$

$$\rho\Big(\frac{\partial u}{\partial t}+u\frac{\partial u}{\partial x}+v\frac{\partial u}{\partial y}\Big)=-\frac{\partial p}{\partial x}+\mu\nabla^2 u-\frac{\mu\epsilon^+}{K}u-\frac{F\epsilon^{+^2}}{\sqrt{K}}|V|u-\frac{\sigma\beta_0^2}{\epsilon\rho}u \tag{2}$$

$$\rho\Big(\frac{\partial v}{\partial t}+u\frac{\partial v}{\partial x}+v\frac{\partial v}{\partial y}\Big)=-\frac{\partial p}{\partial x}+\mu\nabla^2 v-\frac{\mu\epsilon^+}{K}v-\frac{F\epsilon^{+^2}}{\sqrt{K}}|V|v+g\beta(T-T_c) \tag{3}$$

$$\frac{\partial T}{\partial t}+u\frac{\partial T}{\partial x}+v\frac{\partial T}{\partial y}=\frac{k}{\rho c_\rho}\nabla^2 T-\frac{1}{\rho c_\rho}\Big[\frac{\partial q_r}{\partial x}+\frac{\partial q_r}{\partial y}\Big]+\frac{\mu}{\rho c_\rho K}|V|^2+\frac{\sigma\beta_0^2}{\epsilon\rho c_\rho}u^2 \tag{4}$$

where $(u,v)$ are considered dimensional velocity related to components along the $(x,y)$ Cartesian coordinate. $p$ is the pressure, $T$ the local temperature. The density $(\rho)$, dynamic viscosity $(\mu)$, specific heat $(c_\rho)$, time in dimensional form $t$ , and thermal conduction $(k)$. The radiations terms in both x and y are given as $q_{rx}=-\frac{4\sigma^*}{3K'}\frac{\partial T^4}{\partial x}$ and $q_{ry}=-\frac{4\sigma^*}{3K'}\frac{\partial T^4}{\partial y}$, where $K'$ represents absorption coefficient and $\sigma^*$ the Stefan-Boltzmann constant. Using expansion of Taylor series on $T^4$ about $T_c$ and dropping high order terms we have $T^4\approx 4TT_c^3-3T_c^4$. The magnetic field is given as $\frac{\sigma\beta_0^2}{\epsilon\rho}$, where $\sigma$ and $\beta_0$ are the constant impose externally on the magnet. $K=\frac{d^2\epsilon^3}{(150[(1-\epsilon)]^2}$ is the permeability of the porous system, with $d$ being the mean particle diameter, the porosity $\epsilon$ is classified as the fraction of entire volume in void space. $F=\frac{(1.75(1-\epsilon))}{(d\epsilon^3)}$ is the form drag constant, the constant $\frac{F}{\sqrt{K}}$ is the Forchheimer number. The norm of the velocity vector $|V|=\sqrt{u^2+v^2}$, $\beta$ represents thermal expansion (coefficient) and $g$ represents gravitational acceleration.

The viscous dissipation $\phi$ is express as

$$\phi=2\Big[\Big(\frac{\partial u}{\partial x}\Big)^2+\Big(\frac{\partial v}{\partial y}\Big)^2\Big]+\Big(\frac{\partial v}{\partial x}+\frac{\partial u}{\partial y}\Big)^2 \tag{5}$$

Equation 6 shows the dimensionless parameters

$$X=\frac{x}{l},\quad Y=\frac{y}{l},\quad \tau=\frac{\nu}{l^2}t,\quad \theta=\frac{T-T_c}{T_h-T_c},\quad u=\frac{\nu}{H}U,\quad v=\frac{\nu}{l}V,\quad P=\frac{l^2}{\rho\nu^2}p \tag{6}$$

We apply the dimensionless parameter given in Eq.(6) to the the governing equation from Eq.(1)-(4) to obtained Eq.(7)-(10).

$$\frac{\partial U}{\partial X}+\frac{\partial V}{\partial Y}=0 \tag{7}$$

$$\frac{\partial U}{\partial \tau}+U\frac{\partial U}{\partial X}+V\frac{\partial U}{\partial Y}=-\frac{\partial P}{\partial X}+\nabla^2 U-\gamma U-\Gamma|V|U-Ha^2U \tag{8}$$

$$\frac{\partial V}{\partial \tau} + U\frac{\partial V}{\partial X} + V\frac{\partial V}{\partial Y} = -\frac{\partial P}{\partial Y} + \nabla^2 V - \gamma V - \Gamma|V|V + Gr\theta \tag{9}$$

$$\frac{\partial \theta}{\partial \tau} + U\frac{\partial \theta}{\partial X} + V\frac{\partial \theta}{\partial Y} = \frac{1}{Pr}\Big(1 + \frac{4}{3}Rd\Big)\nabla^2\theta + \gamma Ec|V|^2 + Ec\Phi + Ha^2 EcU^2 \tag{10}$$

where $Ra = \dfrac{l^3 g\beta(T_h - T_c)}{\alpha\nu}$ represents the Rayleigh, $\gamma = \dfrac{l^2\epsilon^+}{K}$ indicates the inverse darcy, $\Gamma = \dfrac{l^2 F\epsilon^{+^2}}{\sqrt{K}}$ is the form drag or Forchheimer, $Gr = \dfrac{Ra}{Pr}$ and $Pr = \frac{\nu}{\alpha}$ are the Grashof and Prandtl. $Da = \dfrac{K}{l^2}$, $Ec = \dfrac{\nu^2}{c_\rho(T_h - T_c)l^2}$, $Ha^2 = \dfrac{\sigma\beta_0^2 l^2}{\epsilon\mu}$ and $Rd = \frac{4\sigma^* T_c^3}{kK'}$ represents Darcy, Eckert, Hartmann and Radiation respectively and $\nabla^2\theta = \Big[\dfrac{\partial^2\theta}{\partial x^2} + \dfrac{\partial^2\theta}{\partial y^2}\Big]$

## 3 Entropy Generation

Entropy generation is the process through which a system's entropy rises over time. It is a measure of a system's irreversibility. Entropy is connected to the conversion of usable energy into waste or heat and happens in a variety of physical, chemical, and thermodynamic processes. The effect of entropy is frequently related with the second rule of thermodynamics, which states that in ideal circumstances, the total entropy of an isolated system always tends to grow or remain constant. Heat transmission across temperature gradients, fluid friction, chemical reactions, and viscous dissipation processes all contribute to generation of Entropy. Eq.(11) to Eq.(13) are the governing equations of entropy with magnet incorporated.

$$S_H = \frac{k}{T_c^2}(\nabla T)^2 - \frac{1}{T_c^2}\Big[\frac{\partial q_r}{\partial x} + \frac{\partial q_r}{\partial y}\Big] + \frac{\sigma\beta_0^2}{\epsilon T_c}u^2 \tag{11}$$

$$S_F = \frac{\mu}{T_c}\phi + \frac{\mu}{KT_c}|V|^2 \tag{12}$$

Since total entropy is the sum of entropy due to heat and entropy due fluid friction ($S_T = S_H + S_F$), Then

$$S_T = \frac{k}{T_c^2}(\nabla T)^2 - \frac{1}{T_c^2}\Big[\frac{\partial q_r}{\partial x} + \frac{\partial q_r}{\partial y}\Big] + \frac{\sigma\beta_0^2}{\epsilon T_c}u^2 + \frac{\mu}{T_c}\phi + \frac{\mu}{KT_c}|V|^2 \tag{13}$$

we apply the dimensionless equation Eq.(6) to Equation (11-13) to obtained to Equation (14- 16)

$$S_H = \Big(1 + \frac{4}{3}Rd\Big)\Big[\Big(\frac{\partial\theta}{\partial x}\Big)^2 + \Big(\frac{\partial\theta}{\partial y}\Big)^2\Big] + Ha^2\bar{E}cU^2 \tag{14}$$

$$S_F = \bar{E}c\Phi + \gamma\bar{E}c|\mathbf{V}|^2 \tag{15}$$

$$S_T = \Big(1 + \frac{4}{3}Rd\Big)\Big[\Big(\frac{\partial\theta}{\partial x}\Big)^2 + \Big(\frac{\partial\theta}{\partial y}\Big)^2\Big] + \bar{E}c\Phi + \gamma\bar{E}c|\mathbf{V}|^2 + Ha^2\bar{E}cU^2 \tag{16}$$

where $\Delta\theta = \frac{T_h - T_c}{T_c}$ the dimensionless temperature difference, $\bar{E}c = \frac{PrEc}{\Delta\theta}$ is the modified Eckert, $\Phi$ is the dimensionless viscous dissipation $|\mathbf{V}| = \sqrt{U^2 + V^2}$. We consider $(\Delta T)^2$ as $\Big[\Big(\frac{\partial T}{\partial x}\Big)^2 + \Big(\frac{\partial T}{\partial y}\Big)^2\Big]$

### 3.0.1 Dimensionlessz Boundary Conditions

$$\psi = 0, \quad \omega = -\frac{\partial^2 \psi}{\partial y^2}, \quad \frac{\partial \theta}{\partial y} = 0 \tag{17}$$

The Nusselt number is used to measure if a fluid layer can transfer heat more effectively through convection or conduction. Nusselt's number, a dimensionless quantity, is used to represent heat transmission is in Eq.18.

$$\mathrm{Nu} = -\Big(1 + \frac{4}{3}Rd\Big)\frac{\partial \theta}{\partial x}\Big|_{x=0} \tag{18}$$

Th average nusselts number is also given as

$$\mathrm{Nu}_{avg} = \int_0^1 Nu dy \tag{19}$$

## 4 Lattice Boltzmann Method Formulation

The LBM which uses the mesoscopic numerical approach will be applied in simulating the fluid flow. The Chapman-Enskog expansion was applied and we consider the two-dimensional with nine velocities model ($D_2Q_9$) to simulate the flow. The distribution function from the Lattice Boltzmann equation in terms of the velocities, $u = (u, v)$ and temperature $\theta$ from Eq.(10)-(14) is express as

$$f_i(x + ci \triangle t, t + \triangle t) = (1 - \frac{1}{\tau_f}) f_i(x,t) + \frac{1}{\tau_f} f_i^{eq}(x,t) + \triangle t \cdot F_i, \tag{20}$$

$$g_i(x + ck \triangle t, t + \triangle t) = \Big(1 - \frac{1}{\tau_g}\Big) g_i(x,t) + \frac{1}{\tau_g} g_i^{eq}(x,t) + \triangle t \cdot G_i, \tag{21}$$

For $i = 1, 2, .....8$.

$\frac{1}{\tau_f}$ and $\frac{1}{\tau_g}$ are the relaxation time for the velocity and temperature, $f_k(x,t)$, and $g_k(x,t)$ classified as the distribution function for the temperature and velocity at time $t$. Similarly, $f_k^{eq}(x,t)$, and $g_k^{eq}(x,t)$ the equilibrium for the velocity $(u, v)$ and temperature $(\theta)$. The external forces on the velocity and temperature distribution functions are $\triangle t \cdot F_k$ and $\triangle t \cdot G_k$ respectively. The macroscopic velocity $\boldsymbol{u} = (u, v)$ and temperature $\theta$, with the density per node, $\rho$ are defined as

$$\sum_{k=0}^{8} f_k = \sum_{k=0}^{8} f_k^{eq} = \rho, \qquad \sum_{k=0}^{8} f_k c_k = \rho \mathbf{u}, \qquad \sum_{k=0}^{8} g_k = \sum_{k=0}^{8} g_k^{eq} = \theta. \tag{22}$$

The relaxation times in relation to the velocity and temperature are

$$\nu = c_s^2 \triangle t \Big(\tau_f - \frac{1}{2}\Big), \tag{23}$$

$$\alpha = c_s^2 \triangle t \Big(\tau_g - \frac{1}{2}\Big), \tag{24}$$

where $\alpha = \frac{i}{\rho c_\rho}$ is the thermal diffusivity, $c_s = \frac{c}{\sqrt{3}}$ the speed of sound and $c = \frac{\triangle x}{\triangle t}$ lattice particles speed, $\triangle x$, the lattice space $\triangle t$ the time steps.

There are several forms of equilibrium distribution functions for different lattices structures. For the D2Q9 model we have the form

$$f_i^{eq} = w_i\rho\Big(1 + \frac{c_k \cdot \boldsymbol{u}}{c_s^2} + \frac{(c_k \cdot \boldsymbol{u})^2}{2c_s^2} - \frac{(\boldsymbol{u} \cdot \boldsymbol{u})^2}{2c_s^2}\Big), \tag{25}$$

$$g_i^{eq} = w_i\rho\Big(1 + \frac{c_k \cdot \boldsymbol{u}}{c_s^2} + \frac{(c_k \cdot \boldsymbol{u})^2}{2c_s^2} - \frac{(\boldsymbol{u} \cdot \boldsymbol{u})^2}{2c_s^2}\Big), \tag{26}$$

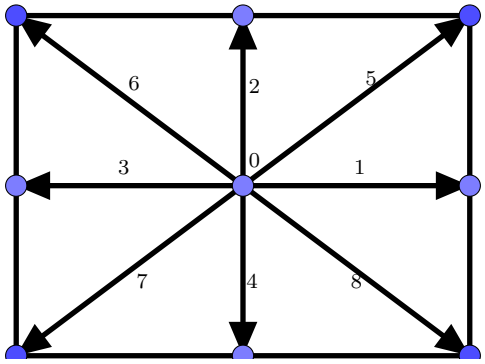


Figure 2: $D_2Q_9$ two-dimensional lattice model

where $c_i$ is the discrete velocities, $\boldsymbol{u} = (u, v)$ velocities on the $x$ and $y$ direction, and the weight function is $w_i$. The discrete velocities and the weight function for a $D_2Q_9$ model is defined as;

$$\mathbf{c}_i = \begin{cases} (0,0) & \text{for} \quad k = 0 \\ \mathrm{c}\Big(\cos\Big[(k-1)\frac{\pi}{2}\Big], \Big(\sin\Big[(k-1)\frac{\pi}{2}\Big]\Big) & \text{for} \quad i = 1,2,3,4 \\ c\sqrt{2}\Big(\cos\Big[(2k-1)\frac{\pi}{2}\Big], \Big(\sin\Big[(2k-1)\frac{\pi}{2}\Big]\Big) & \text{for} \quad i = 5,6,7,8 \end{cases} \tag{27}$$

$$\mathbf{w}_i = \begin{cases} \frac{4}{9} & \text{for} \quad i = 0, \\ \frac{1}{9} & \text{for} \quad i = 1,2,3,4, \\ \frac{1}{36} & \text{for} \quad i = 5,6,7,8. \end{cases} \tag{28}$$

### 4.1 Boundary Condition for the LBM

For the adiabatic walls, the distribution functions remain unchanged at the boundary nodes. while $T_h$ and $T_c$ representing the vertical boundaries can Mathematically be expressed as:

$$f_i(x,y) = f_i(x,y-1) \quad \text{for the top wall}$$

$$f_i(x,y) = f_i(x,y+1) \quad \text{for the bottom wall}$$

$$f_i(x,y) = f_i^{eq}(\rho, u_x = 0, u_y, T = T_h = 1) \quad \text{for the left wall}$$

$$f_i(x,y) = f_i^{eq}(\rho, u_x = 0, u_y, T = T_c = 0) \quad \text{for the right wall} \tag{29}$$

| Gr | Ha | Present | [20] | error[20] |
|---|---|---|---|---|
| $2 \times 10^4$ | 0 | 2.5611 | 2.5665 | 0.0054 |
| | 50 | 1.0982 | 1.0995 | 0.0013 |
| | 100 | 1.0199 | 1.0222 | 0.0023 |
| $2 \times 10^5$ | 0 | 5.0913 | 5.0932 | 0.0019 |
| | 50 | 2.6740 | 2.6791 | 0.0051 |
| | 100 | 1.4588 | 1.4605 | 0.0017 |

**Table 1: Comparison between Nusselt number for present work and Sheikholeslami et al. [20] for Pr = 0.7**

where $f_i$ represents the distribution function for velocity direction i at position (x, y). Here, $f_i^{eq}$ represents the equilibrium distribution function for velocity direction i, which depends on the local macroscopic variables at the boundary nodes, such as density ($\rho$), velocity components ($u_x$, $u_y$), and temperature (T). Setting $u_x = 0$ ensures that the flow is perpendicular to the boundary.

## 5 Code Validation

we compare present results with Sheikholeslami et al. [20] for $G_r = 2 \times 10^4$, $2 \times 10^5$ for Ha values of 0, 50, 100 and results obtained as presented by in Table 1 shows insignificant error for nusselt numbers obtained at different categories to validate the numerical code. Temperature at horizontal mid plane and vertical velocity at vertical mid plane were used to ascertain grid independence for grids of 31 × 31, 41 × 41, 51 × 51, 61 × 61, 71 × 71,81 × 81, 91 × 91 for Ra = 5 × 106, Rd = 2, Ec $= 10^{-6}$, Pr = 0.7, $\gamma = \Gamma = 0.75$, Ha = 0. Figure 3 presents the graphs of the grid independent study adopted.

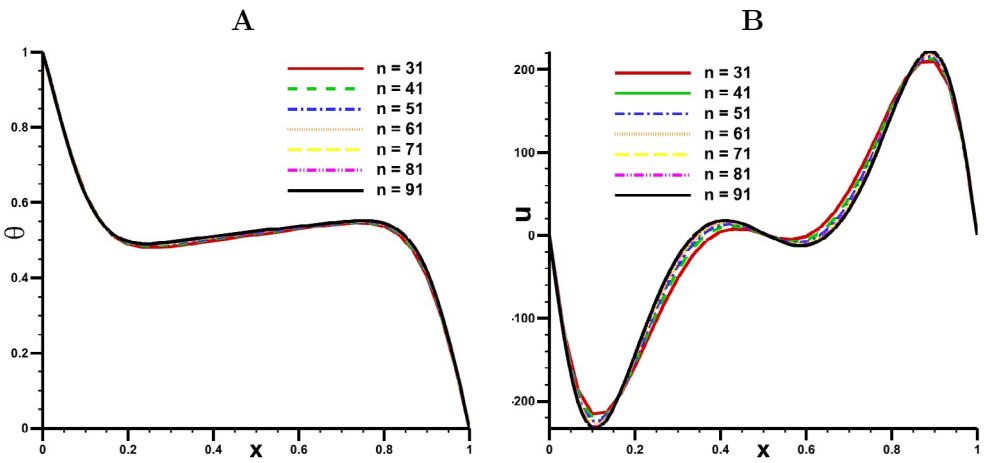


**Figure 3:** A) Temperature at vertical mid plane, B)Vertical velocity at vertical mid plane for Ra = 5 × 106, Rd = 2, Ec = 10−6, Pr = 0.7, $\gamma = \Gamma = 0.75$, Ha = 0

## 6 Results and Conclusion

The effect of Hartmann, Eckert, viscous, and drag forces on streamlines, isotherms, isolines of entropy, time, average and local Nusselt, velocity and maximum streamlines are discussed. The controlling parameter for the investigation include the Grashof ($10^3 \leq Gr \leq 10^6$), the Eckert number ($10^{-6}$, $10^{-5}$, $5 \times 10^{-5}$), the Forchheimer number ($0 \leq \Gamma \leq 10$), inverse Darcy Eckert number ($10^{-6}$, $10^{-5}$, $5 \times 10^{-5}$), the Forchheimer number ($0 \leq \Gamma \leq 10$), inverse Darcy ($0 \leq \gamma \leq 10$), radiation parameter ($0 \leq Rd \leq 10$), Prandtl number Pr (0.7, 1.0, 7.0, 10) and Hartmann number ($10^3 \leq Gr \leq 10^6$). Figure (3-9) shows the results of the effects of the of dimensionless variables on the fluid flow.

### 6.1 Effect of Eckert Number

The Eckert number largely controls energy conversion in the flow, whereas the Hartmann number governs magnetic field behaviour. Figure 4 shows Streamlines ($\psi$), Isotherms ($\theta$) and Isolines of Total Entropy Generation ST at Ra = $10^5$, Pr = 7.0, Ha = 30, Ec = $10^{-6}$, $\gamma = \Gamma = 0.75$ for different Eckert number. Figure 4 shows that streamlines cluster together more as Eckert increases, isotherms appears thesame except for very high Ec which moves the isotherms to the left wall and entropy generation also potraying a similar phenomenum as the isotherms. This behaviour on the fluid is because an increased Eckert numbers are often associated with increased kinetic energy contributions, which can affect flow dynamics and streamline shape. A greater Eckert number indicates that kinetic energy contributes more than thermal energy. This can improve convective heat transfer and mixing efficiency, influencing temperature gradients and isotherm contours. The existence of a magnetic field, as represented by the

Hartmann number, may also change heat transport properties and temperature distribution. The Eckert number influences the energy conversion and dissipation mechanisms, which in turn influences the rate of entropy generation.

Figure 5 shows Vertical velocity along the horizontal mid plane, Total Entropy at the Horizontal mid plane , Local Nusselt number at vertical mid plane for different Ec numbers. The Eckert number affects energy conversion and, as a result, velocity distribution in the flow. Figure 5 shows a convergences at zero after numerous fluid frictions interaction, total entropy is higher as Ec increases and local Nusselt number degrease as Ec is on the rise. The fluid behavior is because kinetic energy dominates flow behaviour, this can result in greater fluid velocities. The Eckert number influences the energy conversion and dissipation processes, which can alter the system's total entropy. Higher Eckert numbers frequently correspond to increased entropy formation as a result of improved mixing and dissipation. The existence of a magnetic field, as denoted by the Hartmann number, might complicate the process of generating entropy. Magnetic fields can influence flow behaviour and modify energy transfer pathways, possibly altering total entropy. The Eckert number influences convective heat transfer through influencing flow dynamics, temperature gradients, and mixing. A higher Eckert number, implying a greater input of kinetic energy, might improve convective heat transport and, as a result, raise the local Nusselt number. The existence of a magnetic field, indicated by the Hartmann number, on the other hand, might affect the heat transport properties and change the local Nusselt number.

Similarly Figure 5 also indicates, Maximum stream function, Average Nusselt number and Total entropy with respect to time. All the variables considered tends to move smoothly as time evolves. The is as a result of the laminar assumptions mentions above. The maximum stream function represents the domain's maximum value for the stream function. The Eckert number influences energy conversion and flow dynamics, which in turn impact velocity distribution and streamline patterns. Increased Eckert numbers are frequently associated with increased fluid velocities and enhanced mixing, which might affect the maximum stream function. The average Nusselt number is the sum of all the local Nusselt values on a particular surface. The Eckert number affects convective heat transfer through influencing energy conversion and flow parameters. As a result, greater Eckert numbers may raise the average Nusselt number. Higher Eckert numbers frequently correspond to increased entropy generation as a result of improved mixing and dissipation. The total entropy of the system may rise or decrease over time, based on the balance of energy inputs, dissipation, and any heat transfer activities that occur in the system.

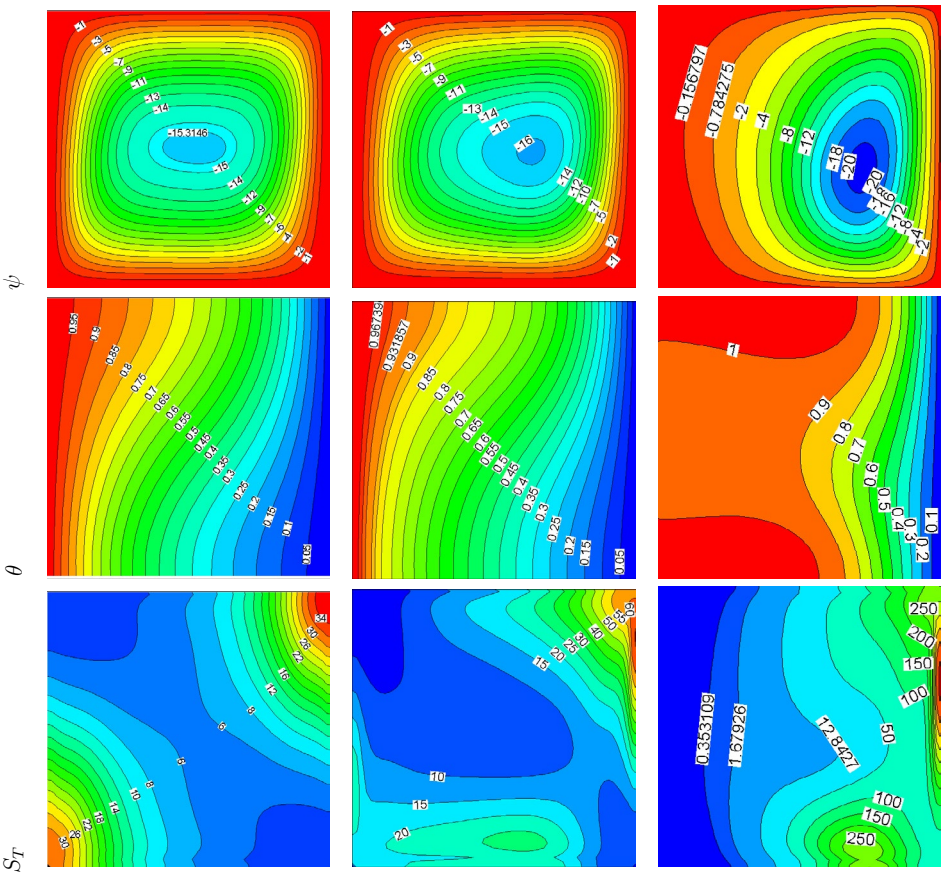


**Figure 4:** Streamlines (ψ), Isotherms (θ) and Isolines of Total Entropy Generation $S_T$ at Ra = $10^5$, Pr = 7.0, Ha = 30, Ec = $10^{-6}$, γ = Γ = 0.75 for (A) Ec = $10^{-6}$ (B) Ec = $10^{-5}$ and (C) Ec = $5 \times 10^{-5}$

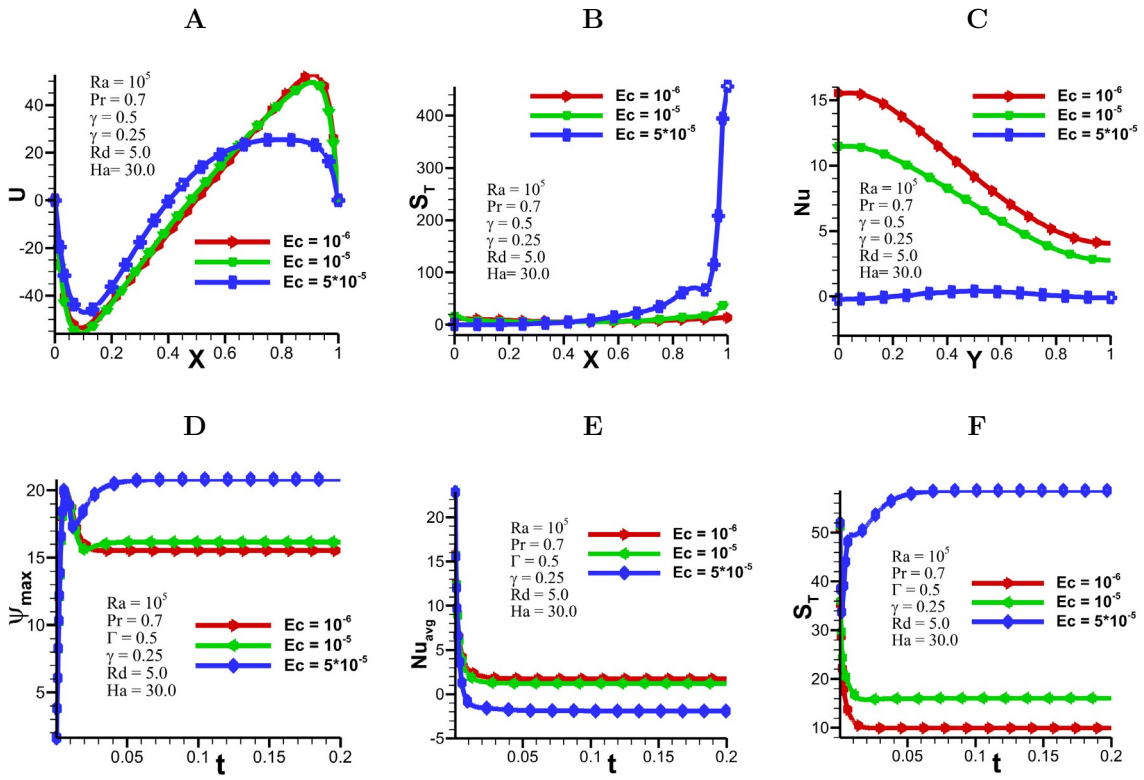


**Figure 5:** A) Vertical velocity along the horizontal mid plane, B) Total Entropy at the Horizontal mid plane C) Local Nusselt number at vertical mid plane D) Maximum stream function E) Average Nusselt number and F) Total entropy

### 6.2 Effect of Hartmann Number

The Hartmann effect tends to restrict conductive fluid mobility perpendicular to magnetic field lines. As a result, the streamlines become increasingly aligned with the direction of the magnetic field. Figure 6 presents Streamlines (ψ), Isotherms (θ) and Isolines of Total Entropy Generation $S_T$ at Ra = $10^6$, Pr = 0.7, Ha = 30, Ec = $10^{-6}$, γ = Γ = 0.75 for different hartmann numbers. The streamlines, isotherms, isolines of entropy tends to appear symmetric due to dominance of the inertia effect as hartmann increase. This alignment causes the fluid to flow following the lines of the magnetic field, resulting in the construction of channel-like flow patterns. Isotherms are lines in a fluid that link places of equal temperature. The existence of the Hartmann effect changes the temperature distribution in the conductive fluid. Cross-field fluid motion suppression restricts mixing and can cause temperature fluctuations along the magnetic field direction. This phenomenon has the potential to deviate from the usual pattern of isotherms found in the absence of a magnetic field. Isolines of entropy are lines that link places with equal entropy, which is a measure of a system's unpredictability. By changing fluid flow and temperature patterns, the Hartmann effect can influence the distribution of entropy in a conductive fluid. Suppression of cross-field motion and changes in temperature distribution can cause aberrations from the normal pattern of entropy isolines found in the absence of a magnetic field.

Figure 7 indicates Vertical velocity along the horizontal mid plane, Total Entropy at the Horizontal mid plane and Local Nusselt number at vertical mid plane. Figure 7 depicts a convergence at zero after several fluid friction interactions, overall entropy increasing as Ha increases, and local Nusselt number decreasing as Ec increases. The local Nusselt number describes the rate of convective heat transport in a fluid at a specific place. By influencing fluid flow and temperature distribution, the Hartmann effect can change the Nusselt number. Because the Hartmann effect inhibits cross-field fluid motion, it can diminish convective heat transfer, resulting in a lower local Nusselt number than in the absence of a magnetic field. A magnetic field perpendicular to the fluid flow can have an effect on the velocity distribution in a conductive fluid. The Hartmann effect dampens fluid velocity perpendicular to magnetic field lines. As a result of this suppression, cross-field velocities are lowered and the velocity component parallel to the magnetic field direction increases. By modifying fluid flow and temperature patterns, the Hartmann effect changes the distribution of entropy. Suppressing cross-field fluid motion can restrict mixing and introduce entropy fluctuations along the magnetic field direction. This phenomenon can cause departures from the usual total entropy pattern seen in the absence of a magnetic field.

Figure 7 shows Maximum stream function, Average Nusselt number and Total entropy with respect to time. As time passes, all of the variables evaluated tend to move smoothly. Which solidifies

the laminar assumption. The Hartmann effect causes fluid flow to align with the direction of the magnetic field, resulting in channel-like flow patterns. The maximal stream function may grow with time as the fluid gets more aligned with the magnetic field. The average Nusselt number denotes the average rate of convective heat transfer in a fluid. The Hartmann effect can minimise convective heat transfer by decreasing cross-field fluid motion. The average Nusselt number may decline with time as the Hartmann effect becomes more powerful. The Hartmann effect can change total entropy by changing the fluid flow and temperature distribution. The total entropy may alter over time owing to variations in fluid motion and temperature patterns generated by the Hartmann effect.

### 6.3 Effect of Grashof Number

In natural convection, the Grashof number influences the flow pattern and the creation of streamlines. Figure 8 shows the effect of different Grashof numbers for on Streamlines , Isotherms and Isolines of Total Entropy Generation at Ra = $10^5$, Pr = 7.0, Ha = 30, Ec = $10^{-6}$, $\gamma = \Gamma = 0.75$ A higher Grashof number indicates stronger buoyant forces and more prominent flow patterns. The flow becomes increasingly chaotic as the Grashof number grows, and the streamlines can display complicated and irregular behaviour. When compared to low Grashof number flows, the flow may form many vortices and eddies, resulting in a more complicated flow pattern. Isotherms are temperature-constant lines in the flow field. The Grashof number determines the form and distribution of isotherms in natural convection. A higher Grashof value results in increased buoyancy and greater heat transfer. As a result, the isotherms are more widely separated, suggesting a greater temperature differential between neighbouring isotherms. As the temperature gradient steepens, the flow may develop more distinct thermal boundary layers. Furthermore, plume formation and temperature stratification can influence the shape and orientation of isotherms in the flow. Entropy isolines in the flow field represent areas of constant entropy. In general, the Grashof number has no direct effect on

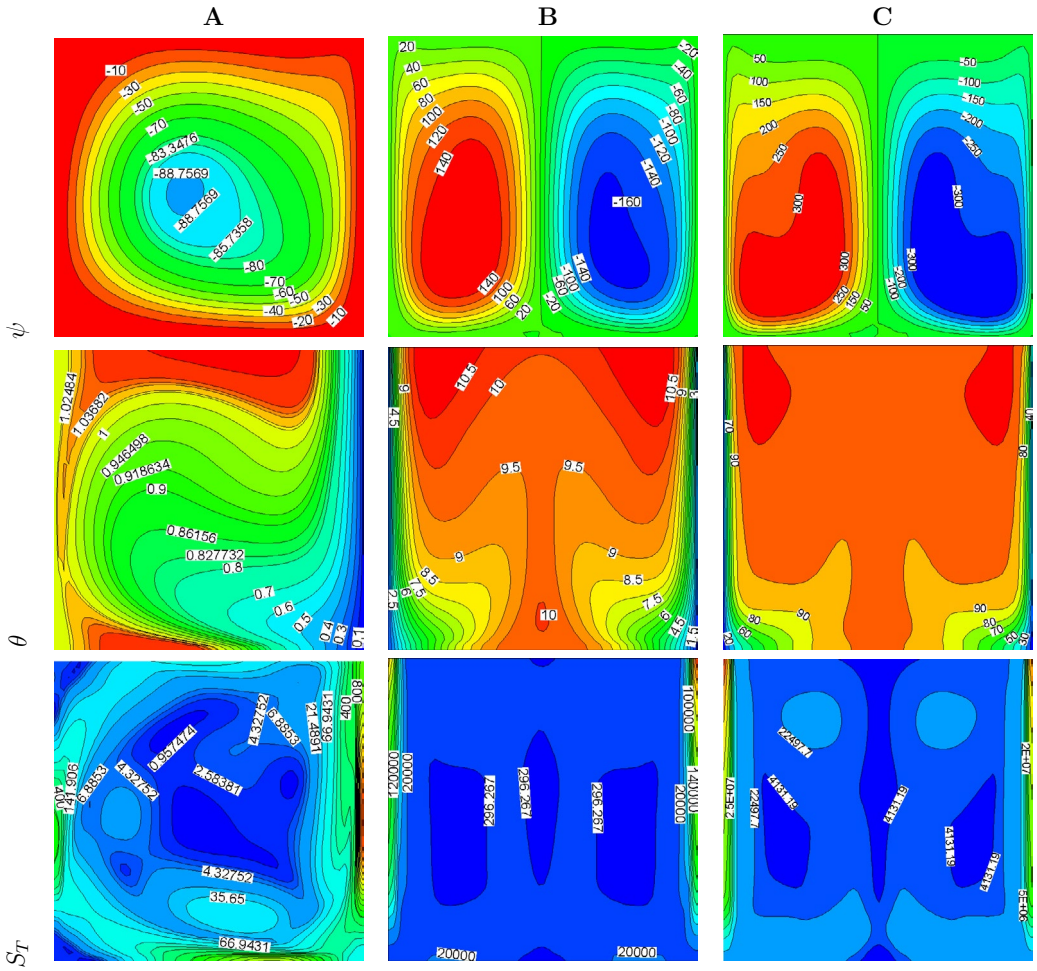


**Figure 6:** Streamlines (ψ), Isotherms (θ) and Isolines of Total Entropy Generation ST at Ra = $10^6$, Pr = 0.7, Ha = 30, Ec = $10^{-6}$, $\gamma = \Gamma =$ 0.75 for (A) Ha = 0 (B) Ha = 30 and (C) Ha = 60

the isolines of entropy. Changes in temperature distribution caused by the Grashof number, on the other hand, can have an indirect effect on the isolines of entropy. Entropy isolines may be more tightly spaced in areas with a strong temperature gradient and buoyancy-induced flow, whereas they may be more widely spread in areas with a smaller temperature difference and less convective motion.

Figure 9 indicates Vertical velocity along the horizontal mid plane, Total Entropy at the Horizontal mid plane and Local Nusselt number at vertical mid plane. The buoyancy forces get greater as the Grashof number increases, resulting to an increase in vertical velocities. Higher Grashof numbers result in improved convective heat transfer, resulting in greater upward or downhill flow velocities depending on the temperature gradient. Particularly in places with considerable temperature variations, the flow may display more violent motion and more vertical mixing. The exact relationship between the Grashof number and vertical velocity is determined

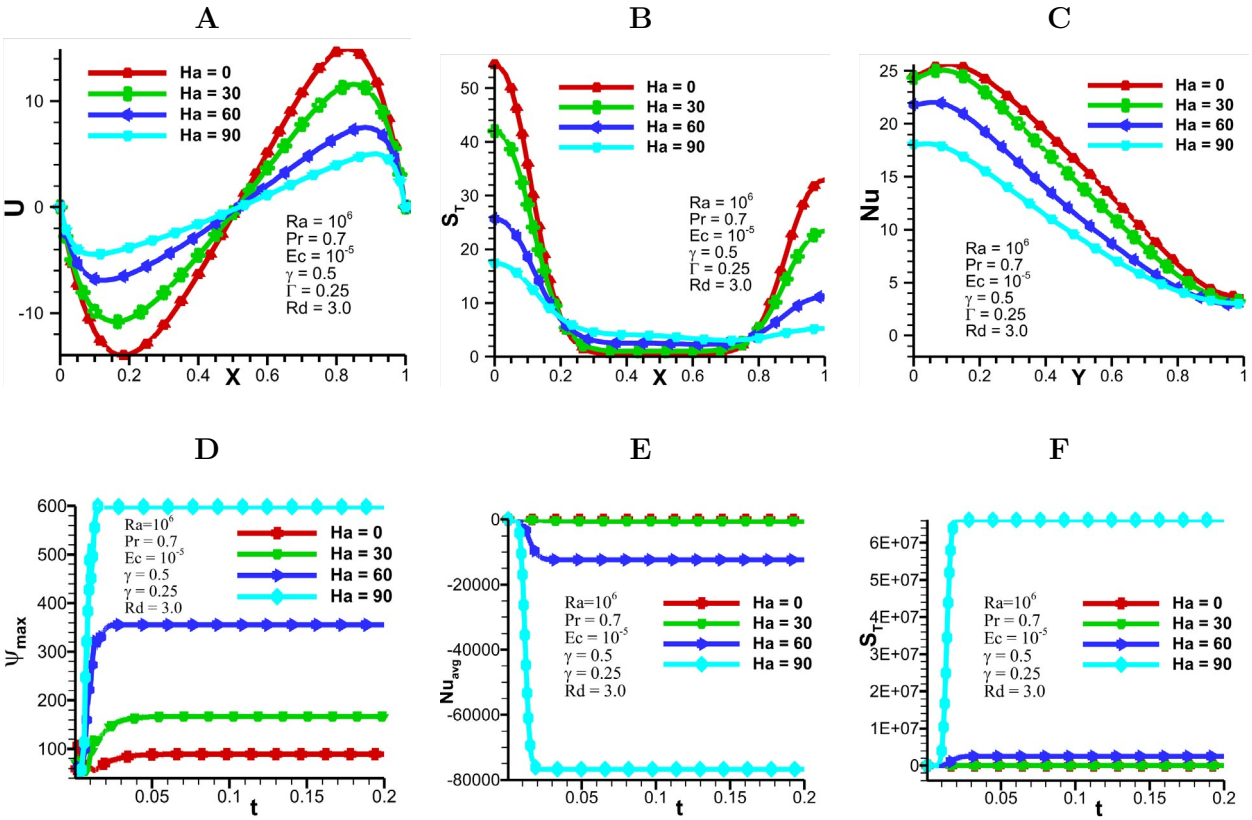


**Figure 7:** A) Vertical velocity along the horizontal mid plane, B) Total Entropy at the Horizontal mid plane C) Local Nusselt number at vertical mid plane D)Maximum stream function E) Average Nusselt number and F) Total entropy

by the flow design and boundary conditions. total entropy is a measure of overall disorder or unpredictability. Changes in the Grashof number can impact the distribution and behavior of entropy in buoyancy-driven flows. Convective heat transfer becomes more prominent as the Grashof number increases, resulting in improved mixing and heat exchange. This can cause changes in the temperature distribution and the production of entropy in the flow. The specific influence of the Grashof number on total entropy is determined on the flow circumstances and the fluid's thermodynamic parameters. Nusselt number (Nu) is a dimensionless quantity that describes the rate of convective heat transport in a fluid. It denotes the proportion of convective to conductive heat transfer. The Grashof number has a substantial influence on the Nusselt number in buoyancy-driven flows. As the Grashof number grows, convective heat transmission takes precedence over conductive heat transfer. This causes the Nusselt number to rise. Higher Grashof numbers correspond to more efficient heat transmission and higher Nusselt numbers. The link between the Grashof and Nusselt numbers is determined by the flow conditions, geometry, and boundary conditions.

Figure 9 shows Maximum stream function, Average Nusselt number and Total entropy with respect to time. The Grashof number can impact the creation and evolution of the streamlines over time. When the flow begins or the temperature gradient changes, the streamlines may shift and create a new flow pattern. The buoyancy forces get greater as the Grashof number increases, resulting in more substantial changes in the flow pattern over time. The flow may display complicated behaviour, such as vortices forming and dissolving, changes in flow recirculation zones, and

changes in overall flow structure. The average Nusselt number describes the rate of convective heat transfer in a fluid system. The Grashof number can influence the evolution of the average Nusselt number as time passes in buoyancy-driven flows. When the flow begins or the temperature distribution changes, the convective heat transfer and hence the average Nusselt number may exhibit transitory behaviour. As time passes, the flow settles into a more steady-state state in which the average Nusselt number approaches a somewhat constant value. The development of the average Nusselt number through time is determined by the flow parameters, geometry, and boundary conditions. total entropy is a measure of overall disorder or unpredictability. In buoyancy-driven flows, the Grashof number can impact the evolution of total entropy over time. When the flow begins or when the temperature distribution changes, the entropy distribution may alter and exhibit transitory behaviour. Convective heat transfer and mixing in the flow can cause changes in the entropy distribution as time passes. The particular evolution of total entropy over time is determined by the flow circumstances, fluid thermodynamic parameters, and the level of mixing and heat exchange.

## 7 Conclusion

The purpose of this study was to evaluate natural convection combining the Lattice Boltzmann Method (LBM) with the Darcy-Forchheimer model to analyse entropy generation in the presence of a partial magnetic influence. Several major discoveries have been gained through extensive numerical simulations and analysis, shedding light on the intricate interplay between fluid flow, heat transfer, and entropy generation in magnetic convection systems. The results show that the Darcy-Forchheimer model helps to predicts the velocity and total entropy in the natural convection process. The addition of a partial magnetic effect caused considerable changes in the fluid flow and heat transfer properties, resulting in large changes in the entropy generation distribution throughout the system. The system's irreversibility was shown to be influenced by a number of parameters, such as Hartmann, Eckert number, and the strength of the magnetic field. The effect of the form and viscous drag number on the generation of entropy was also looked at, and the results showed a shift from predominantly thermal irreversibility to increasingly fluid frictional losses. These findings add to a better understanding of the fundamental mechanisms that drive natural convection with a partial magnetic impact, and they give useful insights to the application of heat transfer systems in the presence of magnetic fields. The LBM, in combination with the Darcy-Forchheimer model, is a strong instrument for modelling and analysing such complicated events, providing its computationally efficient and accurate approach [22].

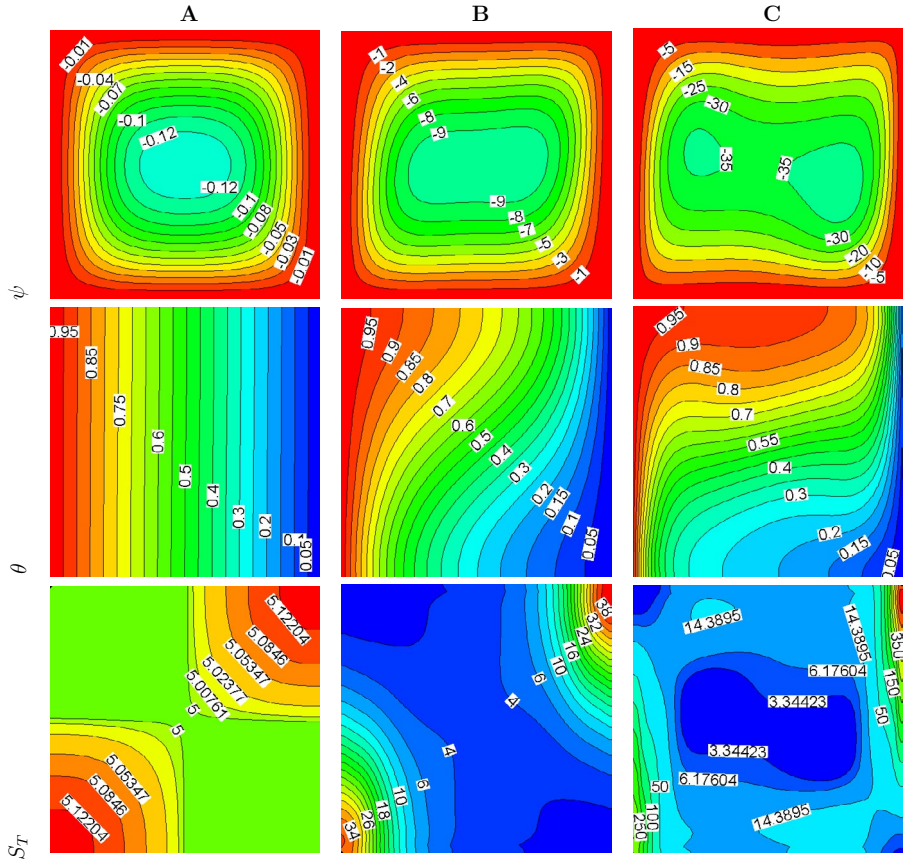


**Figure 8:** Streamlines (ψ), Isotherms (θ) and Isolines of Total Entropy Generation ST at Rd = 3, Pr = 1.0, Ha = 30, Ec = $10^{-6}$, γ = 0.25, Γ = 0.5 for (A) Gr = $10^3$ (B) Gr = $10^5$ and (C) Gr = $10^6$

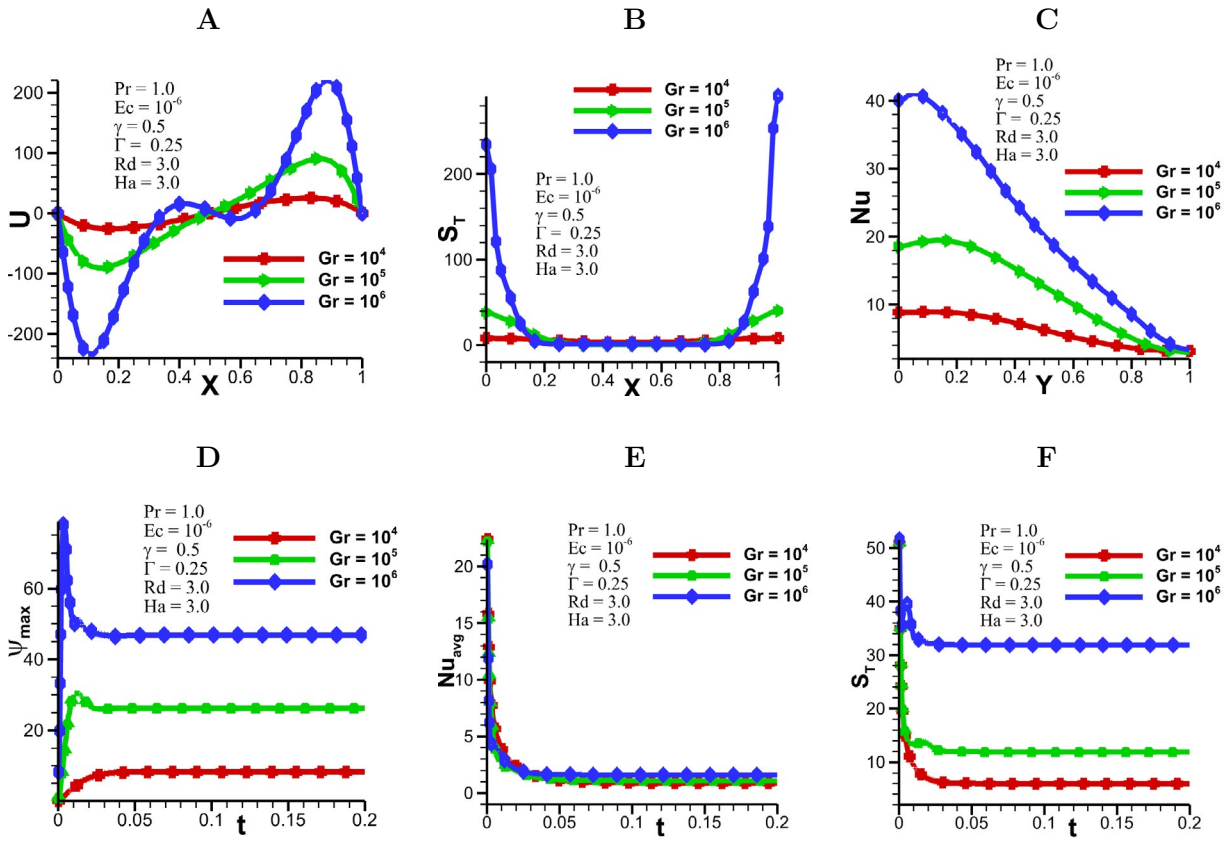


**Figure 9:** A) Vertical velocity along the horizontal mid plane, B) Total Entropy at the Horizontal mid plane C) Local Nusselt number at vertical mid plane D) Maximum stream function E) Average Nusselt number and F) Total entropy

## References


1. Haghshenas, A., Nasr, M. R., & Rahimian, M. H. (2010). Numerical simulation of natural convection in an open-ended square cavity filled with porous medium by lattice Boltzmann method. International Communications in Heat and Mass Transfer, 37(10), 1513-1519.
2. Venkatadri, K., & Bég, O. A. (2022). Lattice Boltzmann simulation of thermo-magnetic natural convection in an enclosure partially filled with a porous medium. Waves in Random and Complex Media, 1-28.
3. Yang, W., & Li, C. (2022). A Unified Lattice Boltzmann Model for Fourth Order Partial Differential Equations with Variable Coefficients. Entropy, 24(9), 1176.
4. Yong, S., & Zhao, W. (2022). A low-storage adjoint lattice Boltzmann method for the control of incompressible flows. Physics of Fluids, 34(9).
5. Geridonmez, B. P., & Oztop, H. F. (2019). Natural convection in a cavity filled with porous medium under the effect of a partial magnetic field. International Journal of Mechanical Sciences, 161, 105077.
6. Mahmoudi, A. (2019). A scale analysis for natural convection in a porous media in the presence of a magnetic field. Journal of the Taiwan Institute of Chemical Engineers, 95, 21-31.
7. Jamshed, W., Gowda, R. J. P., Kumar, R. N., Prasannakumara, B. C., Nisar, K. S., Mahmoud, O., ... & Pasha, A. A. (2022). Entropy production simulation of second-grade magnetic nanomaterials flowing across an expanding surface with viscidness dissipative flux. Nanotechnology Reviews, 11(1), 2814-2826.
8. Tayebi, T., Dogonchi, A. S., Karimi, N., Ge-JiLe, H., Chamkha, A. J., & Elmasry, Y. (2021). Thermo-economic and entropy generation analyses of magnetic natural convective flow in a nanofluid-filled annular enclosure fitted with fins. Sustainable Energy Technologies and Assessments, 46, 101274.
9. Rasool, G., Chamkha, A. J., Muhammad, T., Shafiq, A., & Khan, I. (2020). Darcy-Forchheimer relation in Casson type MHD nanofluid flow over non-linear stretching surface. Propulsion and Power Research, 9(2), 159-168.
10. Loganathan, K., Alessa, N., Tamilvanan, K., & Alshammari, F. S. (2021). Significances of Darcy–Forchheimer porous medium in third-grade nanofluid flow with entropy features. The European Physical Journal Special Topics, 230, 1293-1305.
11. Shah, Z., McCash, L. B., Dawar, A., & Bonyah, E. (2020). Entropy optimization in Darcy–Forchheimer MHD flow of water based copper and silver nanofluids with Joule heating and viscous dissipation effects. AIP Advances, 10(6).
12. Hayat, T., Iqbal, I., Khan, S. A., & Alsaedi, A. (2023). Entropy optimized chemical reactive Darcy–Forchheimer flow of unsteady viscous fluid with magnetic field. Proceedings of

the Institution of Mechanical Engineers, Part E: Journal of Process Mechanical Engineering, 237(3), 928-935.
13. Bouabid, M., Hidouri, N., Magherbi, M., & Brahim, A. B. (2011). Analysis of the magnetic field effect on entropy generation at thermosolutal convection in a square cavity. Entropy, 13(5), 1034-1054.
14. Arikoglu, A., Ozkol, I., & Komurgoz, G. (2008). Effect of slip on entropy generation in a single rotating disk in MHD flow. Applied Energy, 85(12), 1225-1236.
15. Saleem, M., Hossain, M. A., Mahmud, S., & Pop, I. (2011). Entropy generation in Marangoni convection flow of heated fluid in an open ended cavity. International Journal of Heat and Mass Transfer, 54(21-22), 4473-4484.
16. Sciacovelli, A., Verda, V., & Sciubba, E. (2015). Entropy generation analysis as a design tool—A review. Renewable and Sustainable Energy Reviews, 43, 1167-1181.
17. Shojaeian, M., & Koşar, A. (2014). Convective heat transfer and entropy generation analysis on Newtonian and non-Newtonian fluid flows between parallel-plates under slip boundary conditions. International Journal of Heat and Mass Transfer, 70, 664-673.
18. Kiyasatfar, M. (2018). Convective heat transfer and entropy generation analysis of non-Newtonian power-law fluid flows in parallel-plate and circular microchannels under slip boundary conditions. International Journal of Thermal Sciences, 128, 15-27.
19. Zeeshan. (2022). Second law and entropy generation analysis of magnetized viscous fluid flow over a permeable expandable sheet with nonlinear thermal radiation: Brownian and thermophoresis effect. Advances in Mechanical Engineering, 14(1), 16878140221075295.
20. Alzahrani, F., & Khan, M. I. (2022). Entropy generation and Joule heating applications for Darcy Forchheimer flow of Ree-Eyring nanofluid due to double rotating disks with artificial neural network. Alexandria Engineering Journal, 61(5), 3679-3689.
21. Jawad, M., Saeed, A., Khan, A., & Islam, S. (2021). MHD bioconvection Darcy-Forchheimer flow of Casson nanofluid over a rotating disk with entropy optimization. Heat Transfer, 50(3), 2168-2196.
22. Sheikholeslami, M., & Vajravelu, K. (2018). Lattice Boltzmann method for nanofluid flow in a porous cavity with heat sources and magnetic field. Chinese Journal of Physics, 56(4), 1578-1587.